PREDICTIVE THERMAL ANALYSIS OF THE COMBAT SENTINEL SATELLITE

Blake A. Moffitt
Dr. J. Clair Batty (Advisor)

Department of Mechanical and Aerospace Engineering
Utah State University, Logan, UT 84322-1600

ABSTRACT

One of the major technical challenges facing small satellites in low earth orbit is the design of an adequate thermal control system. As the mass of a satellite decreases, the satellite becomes increasingly vulnerable to temperature changes induced by varying orbital heat loads. In order to assure that on-orbit satellite component temperatures are maintained within manufacturing limits, satellite heat transfer must be accurately modeled during the design and analysis of any small satellite. This paper addresses thermal modeling used during the design and analysis of the Combat Sentinel Satellite (CSSAT). An overview of the analysis used to make design decisions and create working thermal models is discussed. A thermal model of the satellite developed using SDRC I-deas Thermal Model Generator (TMG) is also explained. Results from thermal vacuum chamber (TVAC) tests are presented and compared to the analysis. Finally, the correlated thermal model is used to predict temperatures during extreme orbital heating environments.

1.0 INTRODUCTION

As technology advances, the capability of small satellites is increasing. This increasing capability is allowing more complex missions to be performed by satellites that are decreasing in volume and mass. Unfortunately, as satellites decrease in mass, the thermal inertia of the satellite also decreases. This decrease in thermal inertia causes small satellite to be subjected to more severe on orbit temperature swings than larger satellites of the past. These temperature swings are further increased by the growing trend of mounting solar cell arrays on the body of the spacecraft as opposed to using extendable panels. As a result, the thermal control system for small spacecraft must play a primary role in determining the final satellite design. In order for this thermal control system to be successful, accurate thermal modeling must be performed throughout the design and testing of the satellite.

One of the recent satellite programs that has focused on small satellite thermal analysis is the Combat Sentinel program. Combat Sentinel is funded by the Air Force Space Battle Lab (AFSBL) based in Colorado Springs, Colorado. The Space Dynamics Lab (SDL) in Logan, UT was contracted under the Combat Sentinel program to provide a small satellite for use as a thermal test article. SDL was also contracted to build and calibrate a detailed thermal model to be used during the TVAC testing of the satellite.

This paper describes the thermal analysis that was used to develop the final calibrated thermal model of the Combat Sentinel satellite. Several steps of the analysis are discussed that aided in development of the thermal model as well as the satellite thermal design. Specific thermal vacuum chamber testing performed at SDL and Air Force facilities are also discussed as pertaining to the thermal analysis of the satellite. Finally, the calibrated thermal model is used to extrapolate expected temperatures for on orbit conditions.

2.0 SATELLITE OVERVIEW

The CSSAT is fundamentally based on the design of the Ionospheric Observation Nanosatellite Formation (ION-F) USUSAT. The external dimensions, structural design, data processing unit, power control system, and command and telemetry systems were all taken from the USUSAT design. Some small modifications of these systems were made during the design. These modifications mainly consisted of removing components that were not required for basic operation of the satellite during testing. The final CSSAT design resembles a simplified USUSAT

consisting of a data processing unit, a power system, a telemetry transmitter, a camera, and a magnetometer. General specifications of the satellite are given in Table 1.

Table 1. Combat Sentinel Specifications

Maximum Diameter	50.165 cm (19.75 inches)
Thickness	15.24 cm (6 inches)
Total Mass	13.6 kg (30 lb)
Solar Cells	Techstar 3-junction Gallium Arsenide (GaAs)
Battery	4500 mAh NiMH

2.1 Thermal Control System

The most noticeable departure from the USUSAT design is in the thermal control system. The AFSBL requested that CSSAT contain external surface coatings that are similar to other larger satellites used by the Air Force Space Command. Specifically, the inclusion of addition temperature sensors, the use of a radiator surface, and the use of multi-layer-insulation (MLI) external blanketing were requested. These requests required changes to the mounting locations of some internal components and also required the addition of internal resistive heaters.

The final thermal design of the CSSAT contains both passive and active thermal control systems (see Table 2). Heat is passively removed from the spacecraft via a Z-93P painted radiator panel. Satellite panels that directly face the earth are externally blanketed using 21 layer aluminized-mylar radiation shields. Components that were attached to structural panels containing solar cell arrays were moved to the bottom radiator panel. This reduced component temperature swings by eliminating a direct heat path to the highly emissive and absorptive solar panel arrays. This also located a majority of the satellite internal components on the radiator panel. This configuration further reduced temperature swings by locating a majority of the satellite thermal inertia in a central location. This configuration also facilitated the removal of excess heat through direct contact to the radiator panel.

During seasonal orbit cycles where the satellite spends a significant time in the earth eclipse, heaters were needed to assure that the battery temperature remained within its operational limits. During the coldest scenario, the addition of 15 Watts of heater power was needed to maintain the battery in its operating regime. To control the addition of the heating power, thermostats were installed.

In addition to the power needed during cold orbit cycles, additional survival heaters were needed during thermal vacuum chamber testing. A second set of resistive heaters powered by an adjustable external power source capable of producing 100 Watts of heating power was installed. This system was used for periods when the satellite spent extensive time in a cryogenically cooled vacuum environment.

Table 2. Combat Sentinel Thermal Control

External Surface Properties	Irridite Aluminum, Solar Cell Arrays, Z-93P, Aluminized Mylar MLI
Temperature Sensors	30 Sensors Maxim-Dallas Semiconductor DS1820
Thermostats	2 Klixon Thermostats #3BTL6-3
On Orbit Heaters	Ohmite #TCH35P100RJ
Survival Heaters	Ohmite #TCH35P100RJ

2.2 External Structure

The external structure of the CSSAT consists of six rectangular side panels and two hexagonal panels (top and bottom panels). All of the panels are made of irridited aluminum 6061-T6. From a vantage point looking into the satellite with the top panel removed, the sides are labeled clockwise from 1 to 6 with side 1 being the closest panel to the electronics enclosure. The top panel contains a solar panel array of 40 solar cells. The bottom panel is painted with Z-93P paint and is connected to the majority of the internal components. Sides 1, 2, and 6 are covered with MLI using an external layer of either aluminized-mylar or beta cloth. Sides 3, 4, and 5 each contain solar arrays with eight solar cells. In addition to the solar cell array, side 3 contains a camera and a G10 mounting boom. An identical G10 mounting boom is also located on side 6.

Figure 1 shows the Combat Sentinel numbering scheme. The lower left picture shows the solar cell arrays on the top, side 3, and side 4 panels. The lower right picture shows the bottom Z-93P panel.

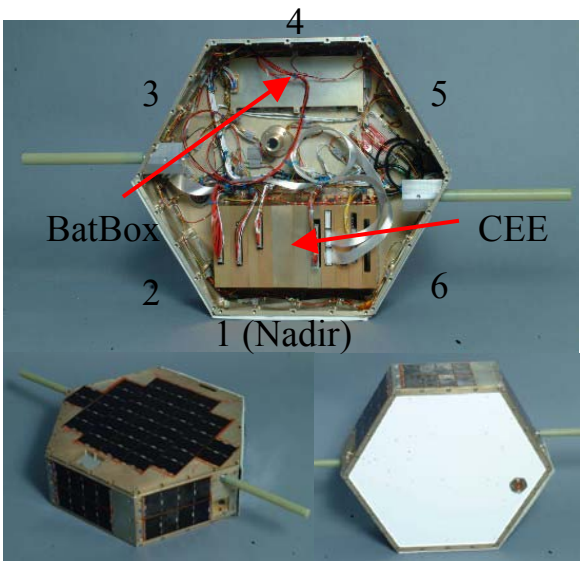

Figure 1. Combat Sentinel panel numbering.

2.3 Orbital Thermal Environment

As a baseline for the design of the Combat Sentinel thermal control system, the orbital conditions defined for the USUSAT were used.

The USUSAT is scheduled for delivery to orbit via the Space Shuttle using the Air Force Multiple Satellite Deployment System (MSDS). Although no specific orbital elements for the USUSAT have been defined, the orbit was assumed to be approximately the same altitude, eccentricity, and inclination as the International Space Station (ISS) orbit. Based on this assumption, the thermal system for the Combat Sentinel test article was designed using environmental heat fluxes common for a low earth orbit (LEO) with an eccentricity equal to zero, an average altitude of 380 km, and an inclination of 51.6 deg. Based on these orbital parameters, the angle between the orbital plane and the solar vector, β, as a function of time was calculated for an entire year. Figure 2 contains the plot of the beta angle calculations.

The extreme thermal environment conditions for the satellite occur at local beta angle extrema as well as beta angles equal to zero. When $\beta = 0°$, the solar vector is parallel to the orbital plane and the satellite experiences a maximum time of approximately 39% of the orbital period in the earth's shadow. This was defined as a cold case orbital scenario. As the beta angle increases, the earth eclipse time decreases. During beta angle extrema, the test article spends a maximum amount of time in the sunlight. For the ISS orbit, the absolute value of beta angles above 70.68° will result in no eclipse. Based on the data in Figure 2, the maximum beta angle for the ISS orbit is approximately 75°. This defines the extreme hot case for the satellite. In order to consider all possible orbital heating conditions for the CSSAT beyond just conditions for the ISS orbit, the hot case orbital scenario was defined when $\beta = 90°$. This condition occurs when the solar vector is normal to the orbital plane.

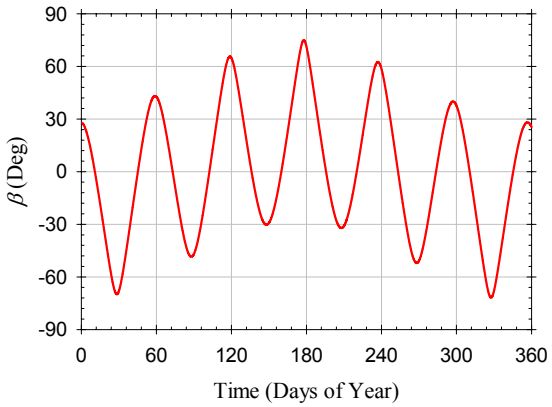

Figure 2. Beta angle variation over one year.

In addition to the beta angles for the hot and cold orbit scenarios, average values for the solar radiation flux, earth IR flux, and albedo factor were needed. These values were based on suggestions contained in several satellite thermal control textbooks[123]. The values used for the analysis are contained in Table 3.

Table 3. Hot and Cold Case Parameters

Hot Case	Cold Case
$\beta = 90°$	$\beta = 0°$
Earth IR = 236 W/m^2	Earth IR = 236 W/m^2
Albedo = 0.4 % of Solar	Albedo = 0.3 % of Solar
Solar = 1370 W/m^2	Solar = 1320 W/m^2
Space Temperature = 4K	Space Temperature = 4K

2.4 Thermal Vacuum Testing Environment

The Wright-Patterson Air Force Base (WPAFB) TVAC chamber was contracted for CSSAT testing. The WPAFB TVAC chamber has a nominal diameter of 23 feet and is 27 feet tall. The chamber is capable of maintaining a temperature of 77 °K at a pressure of 10^{-6} torr.

The satellite was mounted in the chamber using the G-10 mounting booms located on sides 3 and 6. The G-10 booms provide thermal isolation from the mounting mechanism and allow the satellite to be mounted in any orientation relative to the vacuum chamber. An umbilical cable is attached to a port on the bottom panel of the spacecraft to directly communicate with the satellite.

TVAC testing of the satellite began in May 2002. The first tests were designed to allow the satellite to reach an equilibrium temperature with all systems operating. During the tests, heating was accomplished using the externally powered survival heaters mounted on the internal components of the spacecraft. Future testing will study the spacecraft transient temperature response by using a solar source to simulate orbital heating. Although several weeks of testing are planned, at the writing of this paper only the data for the initial equilibrium tests is available for analysis.

3.0 THERMAL ANALYSIS

The main goal of the satellite thermal analysis was to assure that internal satellite components remained within prescribed temperature thresholds (see Table 4). Achieving this goal required accurate modeling of each major component of the satellite. The following section describes the analysis and modeling techniques used to create a working thermal model of the spacecraft. The final detailed thermal model was created using SDRC I-deas Thermal Model Generator (TMG) software.

Table 4. Combat Sentinel component temperature thresholds[4].

Component	Operating Temperature Range (°C)	Survival Temperature Range (°C)
Batteries	0 to 30	-20 to 50
Solar Cells	-100 to 100	-100 to 170
Electronics Enclosure	-40 to 85	-55 to 125
Transmitter	-40 to 85	-40 to 85
Camera	-35 to 65	-40 to 100
Temperature Sensors	-55 to 125	-55 to 125
Magnetometer	-40 to 85	-55 to 125

3.1 Internal Spacecraft Component Analysis

A majority of the Combat Sentinel internal components were designed for the ION-F program. At the onset of the analysis, little information was known about the thermal design of these components. Before attempting to model the entire spacecraft, each component was initially modeled. If possible, actual tests of the components were conducted to aid in the modeling.

3.1.1 Common Electronics Enclosure (CEE)

The Combat Sentinel data processing unit consists of six electronics boards: a central processing unit (CPU) board, a camera board, an input/output (I/O) board, and three power boards. These six boards are enclosed in a series of ten aluminum housings that each attach to a common baseplate. The four empty housings were intended for electronic boards necessary for the USUSAT design but not needed for CSSAT. The entire assembly consisting of the electronic boards, the housings, and the baseplate is referred to as the Common Electronics Enclosure (CEE) (see Figure 3).

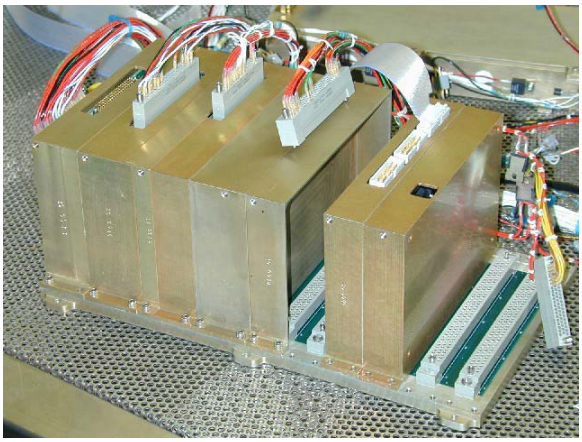

Figure 3. Common Electronics Enclosure. The CEE is shown with some housings removed to allow internal viewing access.

The CEE is designed to remove heat from the electronic boards using several contact points internal to the aluminum housings. The heat then flows from the housings to the heat-sink base plate. The base plate is attached to the bottom of the satellite which radiates the excess heat to space. To increase heat flow across CEE attachment boundaries, 10 mil thick indium foil was used as a thermally conductive gap filler.

Thermal analysis of the CEE began with the electronics boards. After consulting with the electrical engineers on the project, the electronic board components generating the most power were identified. These components were then thermally

modeled using non-geometric (lumped capacitance) elements. Heat dissipated was calculated using voltage and current readings measured during normal operating conditions of the electronic components. To model heat flow from the electronic components to the aluminum housings, heat transfer coefficients for conduction and radiation were calculated.

The conduction heat transfer coefficient from the electronics components to the aluminum housings was calculated using two series conductances. The first conductance represents heat flow in-plane of the PCB material from the electrical component to the aluminum contact point. This conductance is based on the effective thermal conductivity in-plane of the PCB material. This thermal conductivity, k_{eff}, was calculated as

$$k_{eff} = \sum_{i=1}^{n} k_i t_i \Big/ \sum_{i=1}^{n} t_i \qquad (1)$$

where k_i is the thermal conductivity of layer i, t_i is the thickness of layer i, and n is the total number of layers in the PCB material[56]. The second series conductance is due to a contact resistance between the PCB board and the aluminum housing. This resistance was calculated using correlations obtained by SDL thermal engineers on similar thermal analysis projects.

Since each electronic board is completely enclosed by the its respective aluminum housing, the radiation heat transfer coefficient between the board and the housing can be calculated using the gray body view factor for a two surface enclosure[1]. Since the electronic components typically contained fewer elements than the elements required to geometrically mesh the housings, the gray body view factor was subdivided to account for radiation exchange from a single element to several elements[7].

Each aluminum housing was geometrically meshed based on nominal dimensions of the outer geometry. Cutouts, fillets, and tabs were removed to reduce the number of elements needed to mesh the geometry. A comparison between the actual housing geometry and the TMG mesh is given in Figure 4. The surfaces of the housing were meshed using quadrilateral thin shell elements with a thickness calculated to give the proper thermal capacitance. Each edge of the housing that contacts either the CEE baseplate or another housing was meshed using linear beam elements. These beams were given perimeter areas corresponding to the actual contact area of the interface. The beams were given no mass to avoid adding unwanted thermal capacitance to the housing. The beams of each individual housing were joined to beams of other housings using TMG thermal couplings representing the contact conductance across the interface joint. The conductance joints connecting the housings to each other were calculated using an estimated pressure in conjunction with experimental tables of aluminum-to-aluminum contact coefficients as a function of contact pressure.

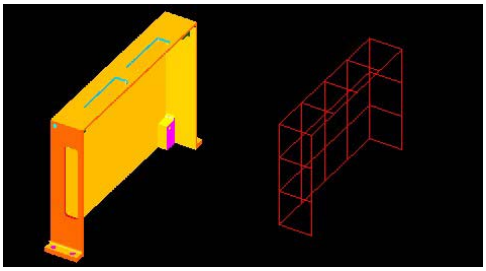

Figure 4. CEE housing mesh.

The base plate of the CEE was meshed as a single flat plate of uniform thickness. The edges of the base plate were meshed with zero mass beam elements similar to the aluminum housing meshes. The perimeter area of these elements was equal to the area of the bolting tabs contained on the bottom of the CEE housings. The beam elements on the bottom of the housing and the edges of the baseplate were then joined using a TMG thermal coupling equivalent to the contact conductance of a joint with indium used as a thermal interface.

To determine the approximate operating temperatures of the electronics vs. their surroundings, the baseplate of the CEE was attached to a constant temperature element maintained at 0° C. The contact conductance between the constant temperature element and the CEE baseplate was calculated assuming indium as an interface filler.

The TMG solution for the heat transfer of the CEE is shown in Figure 5. Figure 5 shows that the heat is predominately flowing down through each individual housing with little heat conducting through the contact joint from one housing to another. Figure 5 also shows that the CEE housing reaches a maximum change in temperature of approximately 2.33° C above the panel that the CEE is attached to.

3.1.2 Battery Enclosure

CSSAT uses a rechargeable battery pack. The battery pack consists of 11 Sanyo Nickel Metal

Hydride (NiMH) 1.2V cells attached in series. The operating temperature range for the battery pack is given in Table 4. Since the batteries have the smallest operating temperature range, most of the thermal design of CSSAT was catered toward maintaining battery operating temperature limits.

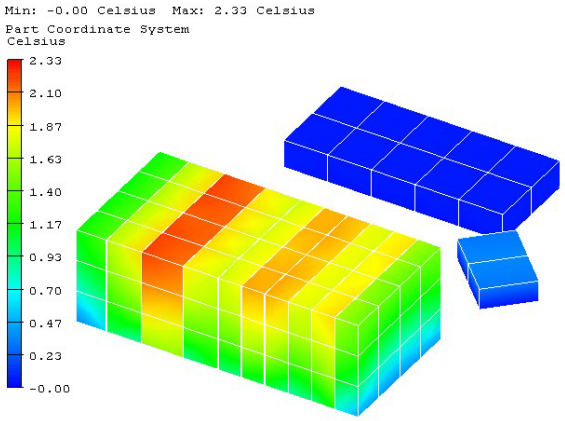

Figure 5. Steady state temperature of the CEE, battery enclosure, and transmitter.

Since the battery manufacturer did not provide SDL with accurate thermal properties of the battery pack, several room temperature vacuum chamber tests were performed.

Determination of battery internal heat generation was achieved by cycling the battery several times in an SDL vacuum chamber. Thermal isolation from the chamber was maintained using a kevlar rope tension support scheme. During testing, the voltage, current, and temperature of the battery pack were monitored (see Figure 6).

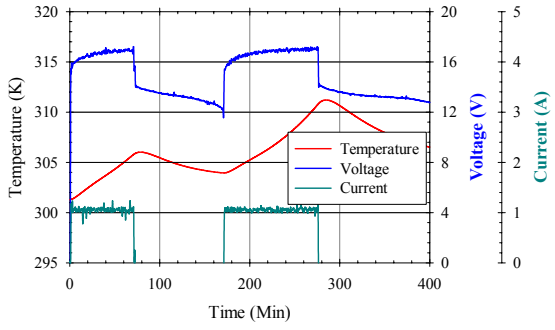

Figure 6. Battery charging and discharging performance.

The test data in Figure 6 shows that as the battery pack is charged, internal heat is generated. In order to determine exactly how much internal heat is generated, the specific heat, C_p, of the battery was needed. The C_p of the battery was calculated by isolating one NiMH cell in an SDL vacuum chamber with a resistive heater attached. The temperature of the cell was recorded as a 0.5 Watt heat load was generated by the heater (see Figure 7).

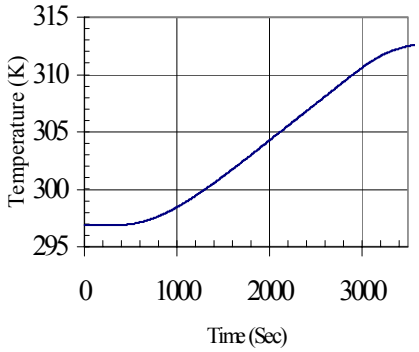

Figure 7. Single battery cell temperature with 0.5 Watt heat load.

Assuming a heat loss to the surroundings of 5% of the total heat load, the battery C_p was calculated to be 1204 J/kg-K. Using this value for the specific heat, the data in Figure 6 reveals that the entire battery pack generates 0.92 Watts while charging.

The battery pack is enclosed in an aluminum box structure with a removable top panel (see Figure 8). The battery box directly attaches to a satellite structural panel using a four-bolt perimeter pattern.

The actually battery pack was thermally modeled using non-geometric elements. The battery box was modeled using four thin shell meshed surfaces in TMG. The meshed surface dimensions were equal to the nominal dimensions of the battery box. As with the CEE, tabs, cutouts, and fillets were not modeled to reduce the number of necessary thin shell elements. A TMG interface thermal coupling was used to add a thermal contact resistance between neighboring elements on the side and top panels. The non-geometric battery element was connected to every element in the battery box using a conductance based on conduction and radiation exchange between the battery pack and the battery box. For the solution process, the battery pack base was attached to a 0° constant temperature boundary element. The resulting solution reveals that in steady state operation, the battery temperature is within 0.25°C of the mounting panel temperature.

Figure 8. View of the battery, the battery box with the top removed, and the transmitter.

3.1.3 Telemetry Transmitter

The CSSAT telemetry communications are handled by an Aydin 2.2 GHz transmitter (TX). During initial tests of the transmitter, heating was found to be uniform over all the surfaces of the transmitter. As a result, the transmitter was modeled using a single non-geometric element. Since the transmitter runs the potential of heating the satellite when turned on, the outside surface geometry of the transmitter was modeled using zero-mass thin shell elements. These elements allow for radiation heat exchange between the satellite and the transmitter but do not add to the thermal capacitance of the transmitter element.

Since the transmitter dissipates a lot of power during normal operation, indium was used to increase heat transfer between the transmitter and its mounting panel. A steady state solution for the transmitter was conducted in the same manner as for the CEE and the battery enclosure. The solution revealed that the equilibrium transmitter temperature is 0.33 °C above its mounting panel (see Figure 5).

3.1.4 Magnetometer, Camera, and Attachment Booms

Other internal components of the CSSAT include a camera, magnetometer, and two attachment booms. The camera was modeled using a box of approximately the same surface dimensions and mass of the camera assembly. The magnetometer was meshed with thin shell meshes applied on the actual housing geometry. The attachment booms also used thin shell elements placed on the actual geometry. All of these components were allowed to directly share nodes with their boundary panels. This allows TMG to calculate a direct conduction path. Contact resistances were added by applying interface thermal couplings to beam meshes located at the boundaries.

3.2 Thermal Modeling of Structural Panels

The structural panels of the spacecraft were modeled using both internal and external thin shell meshes. The two meshes were required since the surface properties vary on the external surfaces of the satellite. The internal mesh of the panels was used to model internal radiation exchange and conduction through the panels. The external panel mesh was created solely to calculate radiation exchange with the space environment.

Internal panel meshing began with attachment surfaces. Attachment surface meshes were created to mirror the baseplate of attaching components. By exactly mirroring these attachments, no error was introduced in joining internal component elements to the panels of the satellite. Once the mesh size for the attachment points was defined, sections of the internal panels directly behind the solar cell arrays were meshed. Once these areas were meshed, elements were created to mesh the remainder of the panels.

Elements of the internal mesh were created using an equivalent thickness. The equivalent thickness was calculated to make the total mass of the panel correct. This allowed the thermal inertia of the satellite to be accurately modeled. Element boundaries located on the edge between panels were meshed with beam elements of zero mass. These elements were used in conjunction with a TMG interface thermal coupling to model the contact resistance between the bolted joints of the panels.

The external panel mesh was created by directly projecting a copy of the internal mesh a short distance into space. These elements were then modified to have no thickness. This allows the elements to participate in radiation heat transfer without contributing extra mass to the satellite.

The radiation properties for the solar cells portions of the external mesh were obtained from the solar cell manufacturer. To account for electrical energy generated by the cells, the absorptivity of the solar array was adjusted based on the efficiency of the solar cells[8].

The solar cell external elements were attached to the internal mesh using a thermal coupling that accounted for a contact resistance caused by Kapton tape and epoxy used to attach the cells to their structural panels. The external aluminum elements were directly attached to the internal mesh without the addition of any contact resistance.

3.3 Small Scale Orbital Thermal Model

One of the key phases of the thermal analysis was the construction of a 13-element model of the spacecraft. This model dedicated one lumped capacitance element for each of the eight panels of the spacecraft. The remaining five elements were used to model the CEE, the battery box, the battery pack, the camera, and the transmitter. Differential equations for each of the 13 elements were derived by performing a heat balance on each element. The general heat balance equation for element i coupled with elements j through n is

$$m_i C_{p_i} \frac{dT_i}{dt} = -\sigma \varepsilon_i A_i T_i^4 + \sum_{j=1}^{n} \sigma \Im_{ij} A_i T_j^4 + \sum_{j=1}^{n} G_{ij}\left(T_i - T_j\right) + Q_d + \alpha_i A_i \left(SF_s + fSF_a\right) \quad (2)$$

where m is mass, σ is the Stefan-Boltzman constant, ε is emissivity, A is area, $\Im_{ij}$ is the gray-body view factor from element i to element j, T is temperature, G_{ij} is a linear conductance from element i to element j, Q_d is power input, α is solar absorptivity, S is solar heat flux, F_s is the solar view factor, f is the albedo fraction, and F_a is the view factor from element i to the sunlit portion of the earth (albedo view factor). To simplify the analysis, all radiation exchange internal to the spacecraft was neglected. This kept the model simple enough to be solved using a standard math solver. Solar and Earth view factors were calculated using exact solutions[1]. Albedo view factors were calculated using curve fits to tabulated albedo data.

The differential equations forming the model were generated and solved using Mathematica 4.0. The solution process used a variable-step high order Runge-Kutta integration routine. To check the accuracy of the solution, an identical model was built in TMG. Results obtained by the two models were identical.

The main advantage of the simplified model was that solutions could be obtained rapidly and easily. This allowed studies to be conducted that varied several heat transfer parameters. Results of these studies were used to help calculate heat transfer coefficients that were estimated during creation of both the simplified and TMG thermal models. One of the primary unknowns in the thermal modeling was the contact conductance between the 8 side panels of the satellite. Using the simplified model, the equilibrium temperature in the thermal vacuum chamber environment was calculated as a function of various contact heat transfer coefficients (see Figure 9).

Based on the data in Figure 9, the panel contact coefficient has only a small influence on the equilibrium temperature for values above 1000 W/m^2-K. Since SDL was confident that a coefficient of 1000 W/m^2-K could be met by assuring that panel joints were clean and smooth, no major errors were expected due to incorrect estimation of the contact conductance.

Two other important properties that could not be exactly determined were the effective emissivity (ε*) of the MLI blanketing, and the effective thermal conductivity through the isogrid structural panels. To more closely determine these parameters Figure 10 and Figure 11 were generated.

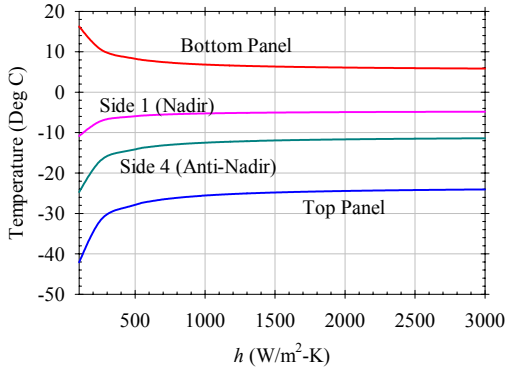

Figure 9. Panel temperature as a function of panel contact coefficient.

Figure 10 displays the equilibrium temperature as a function of ε*. As ε* was varied over a region expected for small blankets, the temperate changed linearly.

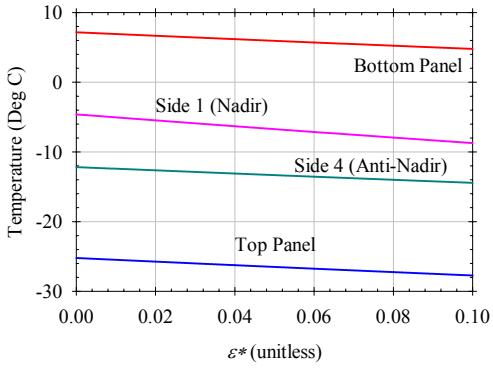

Figure 10. Panel temperature as a function of MLI emissivity.

The most profound temperature variation was found when the thermal conductivity was varied (see Figure 11). As the thermal conductivity was increased above normal values expected for aluminum, the average temperature of the panels containing solar cells increased while the blanketed panels and the radiator panel decreased in temperature. This is a direct result of increasing the linear heat transfer coefficients between the structural panels allowing heat to flow through the satellite with less resistance. The end result is a decrease in localized heating of the satellite.

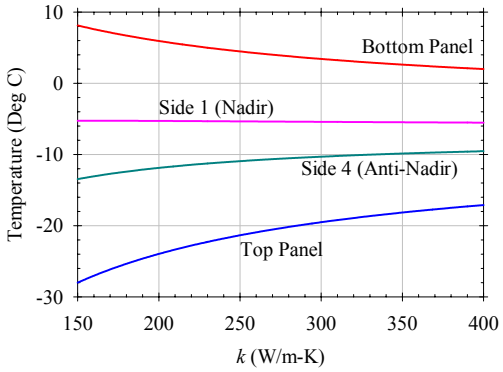

Figure 11. Panel temperature as a function of thermal conductivity.

The initial solution of the model equilibrium temperatures was obtained using $\varepsilon^* = 0.01$ and $k = 177$ W/m-K (see the uncorrelated temperatures in Table 5). Assuming that the other heat transfer parameters used in the model were accurate, calibration required obtaining accurate values of ε^* and k. Rather than systematically adjusting each parameter until an accurate correlation was achieved, a multi-dimensional optimization method was used. Since the curves in Figure 10 and Figure 11 are continuous and differentiable, Newton's method can be easily employed[9]. Since k has the most profound effect on the top panel and ε^* has the most profound effect on the Nadir panel, comparison of these two panel temperatures with the TVAC tests was used to define the following multi-dimensional objective function

$$\vec{f}(\varepsilon^*,k) \equiv \begin{bmatrix} f_1 \\ f_2 \end{bmatrix} \equiv \begin{bmatrix} T_t - T_{ta} \\ T_1 - T_{1a} \end{bmatrix} \qquad (3)$$

where T_t and T_1 are the respective top and side 1 element temperatures, and T_{ta} and T_{1a} are the average panel temperatures measure on the satellite. The solution is obtained by forcing the objecting function to approach 0. This is accomplished by implementing the following partial derivative matrix:

$$\nabla\vec{f}(\varepsilon^*,k) = \begin{bmatrix} df_1/d\varepsilon & df_1/dk \\ df_2/d\varepsilon & df_2/dk \end{bmatrix}. \qquad (4)$$

The Newton iteration is achieved by solving Eq. (5) and substituting the result into Eq. (6).

$$\nabla\vec{f}(\varepsilon^*_i, k_i)\vec{V} = -\vec{f}(\varepsilon^*_i, k_i) \qquad (5)$$

$$\begin{bmatrix} \varepsilon^*_{i+1} \\ k_{i+1} \end{bmatrix} = \begin{bmatrix} \varepsilon^* \\ k \end{bmatrix} + \vec{V} \qquad (6)$$

After two Newton iterations, the updated values were $\varepsilon^* = 0.073$ and $k = 429.0$ W/m-K. The resulting temperatures of the satellite are given in Table 5. The data in Table 5 demonstrates the value of using an optimization scheme for model calibration. After only two iterations varying only two parameters, the total difference between the model temperatures and the average measured temperatures dropped from 41.155 °C to 9.111 °C. Achieving this increase in accuracy required only six executions of the thermal model.

Provided that the objective function is continuous and differentiable, Newton's method can be applied to higher dimensional objective functions to calibrate more parameters at once. The only drawback is that as the number of parameters increases by n, the size of the matrix in Eq. (4) increases to n^2 components. This drastically increases computation time.

The calibrated ε^* in the thermal model is over seven times the initial estimated value. This increase led to a direct investigation of the MLI construction. Since three separate MLI blankets were used to cover sides 1, 2, and 6, the area of each MLI blanket is only 382.26 cm^2. Also, technicians attached the MLI blanketing to the each panel using two strips of Velcro that run the length of the blanket. Sowing the Velcro to the blanket resulted in two extra lines of stitches across each blanket. This extra stitching compiled with the edge effects inherent to the small surface area caused several contact points between the Mylar layers that vastly decreased the performance of the blanket.

The increase in k required for correlation of the model is likely a result of model simplifications. Since each panel as assumed to be isothermal, the

increase in k may account for effects due to temperature gradients across the panels. Another effect may be due to assumptions used to calculate the linear conductances between the elements. To calculate cross sectional areas for the conductances, a uniform thickness was assumed. This thickness is based on maintaining the actual mass of the panel and does not represent the effective thermal cross section of an isogrid panel. The increase in k may also be an indication of heat flow through an isogrid structure as opposed to a flat plate.

Table 5. Steady state model temperature correlation

Element	Uncorrelated Model Temperature (°C)	Correlated Model Temperature (°C)	Actual Temperature (°C)
Side 1	-5.04736	-7.49648	-7.5
Side 2	-5.81391	-7.82946	-7
Side 3	-10.6776	-9.92619	-9
Side 4	-12.4136	-10.7798	-9.5
Side 5	-11.6962	-10.4565	-7.5
Side 6	-6.01429	-7.93602	-6
Top	-25.4891	-18.0698	-17.6
Bottom	6.91463	0.25587	0.6
BatBox	10.87664	4.217893	6.5
CEE	13.81977	7.161082	5
TX	7.91464	1.255883	3
Cam	-9.6776	-8.9262	-6
Total Error	41.155 °C	9.111 °C	

3.4 Internal Spacecraft Radiation Analysis

During development of the simplified thermal model, internal radiation was neglected. To either justify or change this assumption for use in the TMG model, an analysis was performed to determine how much internal radiation heat transfer occurs in the satellite. Internal radiation of the satellite was calculated using a radiation enclosure containing internal spacecraft component meshes as well as the internal mesh of the spacecraft panels.

To understand the radiation exchange internal to the spacecraft, black body view factors were merged to created a set of view factors corresponding to the elements used in the simplified model. View factor merging in TMG is accomplished using the VFMERGE command. Table 6 contains the groupings used for view factor merging.

To model diffuse reflections within the satellite, gray body view factors, $\Im_{ij}$, were used. Calculation of the gray body view factors was performed using Hottel's Zonal Method[10]. The Zonal Method algorithm was written and executed in Mathcad.

$$\Im_{ij} = B_{ij}\varepsilon_i \tag{7}$$

Using Eq. (7), Gebhart radiation exchange factors, B_{ij} were calculated. Although these exchange factors were not needed for the internal radiation analysis, they are typically used to define radiation conductances in heat transfer codes. Using the actual temperatures in Table 5, the radiation exchange between internal elements of the spacecraft was calculated.

Table 6. Internal satellite radiation using the CEE as the primary element.

Secondary Elements (j's)	F_{ij}	B_{ij}	Radiation Exchange (mW)
Side 1	0.180	0.071	-52.373
Side 2	0.106	0.062	-44.524
Side 3	0.027	0.048	-40.165
Side 4	0.023	0.052	-44.580
Side 5	0.033	0.053	-39.882
Side 6	0.104	0.060	-39.974
Top	0.349	0.251	-319.612
Bottom	0.142	0.150	-40.818
BatBox	0.011	0.047	4.532
TX	0.006	0.012	-1.560
Magnetometer	0.008	0.010	-1.717
Boom Side 3	0.003	0.010	-8.542
Boom Side 6	0.004	0.011	-7.042
Camera	0.004	0.012	-7.865
Self	0.000	0.152	0.000
Sum	1.002	1.000	-644.120

Table 6 shows the view factors and net heat exchange between the CEE and the rest of the internal satellite enclosure. During the equilibrium test, only 0.644 Watts of net power is being radiated away from the CEE. Compared to 42.7 Watts of heating power that is directly going into the CEE from the satellite electronic boards and survival heaters, this only accounts for 1.5% of the net heat flow away from the CEE. Since performing internal radiation calculations greatly increases solution times and only accounts for a small percentage of the total heat transfer, internal radiation was ignored.

3.5 Equilibrium Temperature Results

To check the initial accuracy of the TMG model, the TVAC equilibrium temperature test was simulated. To simulate the WPAFB chamber, a black-body radiation enclosure maintained at 77 °K was placed around the satellite. To simulate satellite heaters, heat loads were placed on elements corresponding to heater locations. The heat loads were based on resistance measurements of the CSSAT heater configuration.

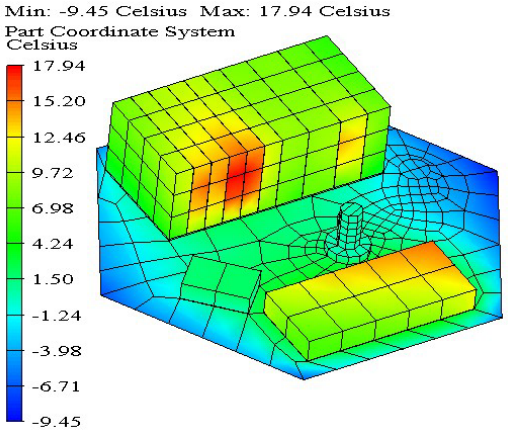

Figure 12. Equilibrium temperature distribution.

The initial results of the TMG solution were excellent. Most of the temperatures were within 1 to 2 °C of the TVAC test results. The only exception was the camera temperature which was 4 °C colder than measured. To calibrate the TMG model, small changes were made to thermal coupling values. In all cases, the initial small errors were due to estimates made calculating contact resistances between components. A comparison of the calibrated TMG model and the test results is given in Table 7.

Table 7. Equilibrium TMG model results.

Component	TMG Temperature (°C)	Actual Temperature (°C)
CPU	22.4	22
I/O Board	16.4	16
Battery 1	8.6	7
Battery 2	8.7	6
CEE 1	6	4
CEE 2	5	5
Transmitter	2.8	3
Camera	-6.4	-6

The equilibrium temperature distribution inside the satellite is shown in Figure 12. This distribution shows the temperature gradients resulting from power provided by the survival heaters. Figure 12 also shows that the temperature gradient across the bottom panel is over 10 °C. Neglecting this large temperature gradient may be one of the reasons that the *k* value in the simplified model had to be increased to correlate the model.

3.6 Orbital Predictions

Once the TMG model was correlated, transient analyses were executed to predict the temperature range of the satellite components. The orbital heating conditions used for these analyses are described in Table 3. Figure 13 shows a TMG orbit visualization of the CSSAT in the both the cold and hot case orbits. For the cold case orbit, the CSSAT is positioned so that the smallest cross section faces the sun. This attitude results in the least amount of satellite heating and is thus the coldest configuration the satellite could ever experience.

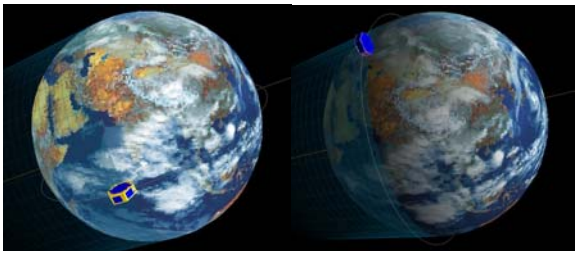

Figure 13. TMG cold (left) and hot (right) case orbits.

The temperature response for several cold case orbits is available in Figure 14. For these orbits the CPU temperature varies approximately 4°C per orbit while the battery temperature varies by about 5 °C.

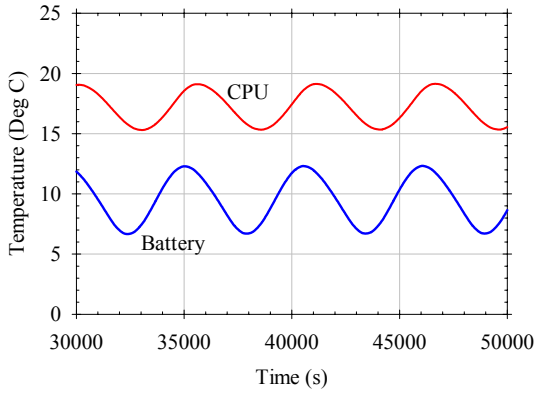

Figure 14. TMG cold case predictions.

The most severe satellite heating occurs when the top side faces the sun for the an entire hot case orbit. For this case, the environmental fluxes are nearly constant and thus a steady state solution can be used to calculate the equilibrium temperature distribution.

The equilibrium temperature distribution for the hot case is shown in Figure 15. In this figure the battery temperature is shown to be below its maximum operating value of 30 °C. One of the main sources of heating for this case is the 25 Watts of excess power created by continuous operation of the transmitter. During a realistic orbit, the transmitter would only be turned on while the satellite is in range of the ground station antenna. For most ground station latitudes, the satellite would only be in antenna range for a few minutes anywhere from 2-5 times a day. With the transmitter on, the batteries will be within 5 °C of their maximum operating limit, but will never exceed their maximum temperature limit.

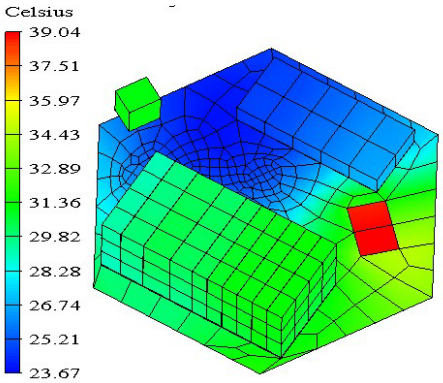

Figure 15. Hot case temperature distribution.

4.0 FURTHER WORK

Transient TVAC tests of CSSAT are scheduled to begin in May of 2002. These tests will monitor the response of the satellite to a simulated solar source. Data will be collected in several different satellite orientations to simulate several orbital scenarios. Once the data is collected, the thermal models of CSSAT will be calibrated to accurately model transient temperature response to orbital heating. Finally, analysis of all test results will be used to increase the understanding of small satellite heat transfer.

5.0 CONCLUSION

Using analysis techniques outlined in the preceding sections, accurate thermal modeling of the CSSAT was achieved. This modeling was verified using measured temperature results from thermal tests performed on CSSAT components as well as TVAC tests of the entire satellite. Using the thermal models of the CSSAT, orbital temperatures for the warmest and coldest possible orbital conditions were predicted. Based on the results of these predictions, the validity of the CSSAT thermal design was established.

6.0 ACKNOWLEGEMENTS

Success in this project would have been very difficult with out the help of several thermal engineers at SDL. The author would like to personally thank Scott Schick, Scott Jensen, and Brett Lloyd for their expertise during the course of this project. In addition, the author would also like to personally thank Lt. Colonel Thomas Shields for use of the CSSAT TVAC test data. Finally, thanks must be given to Dr. Charles Swenson and Dr. Frank Redd for encouraging the writing of this paper.

7.0 REFERENCES

[1] Karam, R., *Satellite Thermal Control for Systems Engineers*, AIAA, Reston, 1998.

[2] Gilmore, D., *Satellite Thermal Control Handbook*, Aerospace Corporation Press, El Segundo, 1994.

[3] Piscane, V. and Moore, R., *Fundamentals of Space Systems*, Oxford University Press, New York, 1994.

[4] Moffitt, B., *Combat Sentinel Spacecraft Qualification and Acceptance Test Plan*, Space Dynamics Lab Internal Document, SDL/02-093, 2002.

[5] Graebner, J.E., *Thermal Conductivity of Printing Wiring Boards*, Technical Brief, Electronics Cooling Magazine, Vol. 1, No.2, October, 1995.

[6] K. Azar and J.E. Graebner, *Experimental Determination of Thermal Conductivity of Printed Wiring Boards*, Proceedings, SEMI-THERM XII Conference, March, 1996

[7] Incropera, D., and DeWitt, D., *Fundamentals of Heat and Mass Transfer*, 4th Edition, John Wiley & Sons, New York, 1996.

[8] Rauschenbach, H. S., *Solar Cell Array Design Handbook*, Van Nostrand Reinhold Company, New York, 1980.

[9] Turner, K., *Newton's Method for Finding an Approximate Local Minimizer*, Class Notes, USU Math 5640, Spring, 2002.

[10] Hottel, H., and A.F. Sarofim, *Radiative Transfer*, McGraw-Hill, New York, 1967.